Reactive Scattering from Brute Force Oriented Asymmetric Top Molecules: $K + C_6H_5I \rightarrow KI + C_6H_5$

H. J. Loesch and J. Möller

Fakultät für Physik, Universität Bielefeld, Universitätsstrasse 25, D-33615 Bielefeld, Germany

Received: March 27, 1997; In Final Form: May 27, 1997[⊗]

In a crossed molecular beam experiment, we have measured angular and time-of-flight (TOF) distributions of products formed in the reaction $K + C_6H_5I \rightarrow KI + C_6H_5$ at a collision energy of $E_{tr} = 1.9$ eV. From these data we have extracted the double-differential reaction cross section in the center-of-mass frame. The brute force technique has been applied to orient for the first time an asymmetric top, namely the reagent molecule C_6H_5I. The effect of molecular orientation on the angular distribution of products has been investigated. We determined the difference of product intensity for (a) preferred encounters with the I end and the phenyl end (parallel steric effect) and (b) side-on attacks with the axis pointing in two opposite directions (perpendicular steric effect). We find (i) preferred sideways scattering of KI with a mean recoil energy of 31.6% of the totally available energy; (ii) an additional reaction channel with a branching ratio of 0.65% by which a flux of slow products, most likely KI, is formed; (iii) the transformation of the data to a more adapted coordinate frame reveals that backward rather than sideways scattering reflects the dynamics of the reaction; (iv) a tight correlation between the direction of the product flux and the orientation of the molecular axis; (v) the experimental results can be rationalized by the direct interaction with product repulsion (DIPR) model; (vi) the ratio of product yield for attacks of the K atoms to the I end (head) and the phenyl end (tail) amounts to ≈28:1; (vii) the full apex angle of the cone-of-acceptance amounts to ≈110°; (viii) the harpooning mechanism and simple molecular orbital arguments rationalize the impulsive reaction mechanism implicit to the DIPR model and offer an explanation for the existence of a channel for slow KI products.

I. Introduction

Moderately strong electric dc fields have been used lately to orient the axes of polar molecules in rotationally cold nozzle beams (brute force technique).[1] First applications of this simple orientation technique were devoted to reactive scattering,[1−4] spectroscopy,[5−7] inelastic scattering,[8] and photodissociation.[9,10] It helped to overcome the restriction to polar symmetric top molecules imposed by the conventional electric hexapole technique[11] and made the investigation of orientation dependent effects to an almost universal tool for the exploration of molecular dynamics.[12] A successful application to reactive scattering from an oriented $^1\Sigma$ diatomic has been reported previously.[3] In the present study the brute force technique is used to measure for the first time orientation effects in reactive collisions with an asymmetric top molecule.

In a series of crossed-beam experiments we have studied reactive scattering of K atoms from several oriented, asymmetric top species, such as halogenated alkanes, alkenes, benzene, and toluene.[13] In this paper we report results for the exoergic reaction

$$K + C_6H_5I \rightarrow KI + C_6H_5 \qquad \Delta D_0 = 0.6 \pm 0.1 \text{ eV} \quad \text{(R1)}$$

The experiments were performed at a collision energy of $E_{tr} = 1.9$ eV.

We have measured an angular distribution and time-of-flight profiles of KI formed in reactions with randomly oriented molecules (orientation field turned off). From these data the double-differential reaction cross section in the center-of-mass (CM) frame was extracted. We find preferred sideways scattering, in contrast to results of an investigation at thermal collision energies where preferred backward scattering was found.[14] In addition to the dominant flux of products a faint, sharply forward scattered component is observed, which consists of slow particles, most likely KI, but other products cannot be excluded as yet. The angular distributions of products measured for reactions with oriented molecules (orientation field on) are markedly influenced by the prepared orientation (steric effects). The parallel steric effect probes the difference of the reactivity for end-on encounters; the findings indicate that attacks to the I end form products favorably. For the first time the perpendicular steric effect has been measured. This quantity characterizes essentially the deviation of the product flux from the cylindrical symmetry around the relative velocity vector. The existence of a nonvanishing perpendicular steric effect as well as the angular dependence of both steric effects manifest a tight correlation between the direction of the product flux and the orientation of the molecular axis. The data are analyzed in terms of the orientation-dependent double-differential reaction cross section which is expanded in a series of real spherical harmonics.[1,15] Our findings allow the determination of the first three moments of the expansion.

The results can be rationalized to a large extent by a model incorporating an impulsive reaction mechanism, namely, the direct interaction with product repulsion (DIPR) model.[16] By application of the DIPR model we find that the ratio of product yields for head (I end) and tail (C_6H_5 end) encounters amounts to around 28:1. Obviously, the phenyl group effectively hinders the initiation of product formation. The steric opacity function decreases steeply with the bond angle of the transition complex C_6H_5-I-K and defines a full apex angle of the cone-of-acceptance of roughly 110°. Furthermore, presentation of the data in a coordinate system adapted to the impulsive mechanism discloses that preferred backward scattering rather than sideways scattering of products is characteristic for the dynamics of R1. This and the other findings point to a tight relationship of R1

[⊗] Abstract published in *Advance ACS Abstracts,* September 15, 1997.

S1089-5639(97)01087-6 CCC: $14.00

TABLE 1: Important Dimensions and Beam Operation Conditions

	K beam	C_6H_5I beam
dimensions		
nozzle diameter (mm)	0.12	0.1
skimmer diameter (mm)	1.0	0.5
nozzle skimmer		
distance (mm)	15	10
fwhm of angular		
beam profile (degree)	1.0	4.5
TOF analyzer: length-of-flight path (mm)	1428/1128	1148/848
stagnation conditions		
vapor pressure (mbar)	3	60
He pressure (mbar)	850	800
nozzle temperature (K)	1045	445
velocity distributions		
v_0 (m/s)	2810	1730
α (m/s)	301	110
$T_{\|\|}$ (K)	213	148
E_{tr} (eV)	190	

and the well-studied reaction K + $CH_3I \rightarrow KI + CH_3$.[17−20] Analogous to the latter an electron transfer from the alkali atom into an antibonding σ*-type molecular orbital of the C−I bond of iodobenzene may cause the rapid dissociation of the reagent molecule into C_6H_5 and I^-. But in contrast to CH_3I the lowest unoccupied molecular orbitals of iodobenzene belong to the π electron system and are localized at the carbon ring. The population of the antibonding σ* orbital and the migration of the electron from the ring to the I atom eventually take place during the separation of the anion.[21]

II. Apparatus

Details of the crossed molecular beam apparatus and the orientation technique have been described elsewhere.[1−3] Briefly, both the K and the iodobenzene beams are created by supersonic expansion through a nozzle and collimated by skimmers; they intersect perpendicularly. The reagents are seeded in He. The beams are monitored by a surface ionization (K) and a mass spectrometer (C_6H_5I) detector. Conventional single pulse TOF technique employing a fast rotating slotted chopper wheel is used to determine the (density) velocity distributions of the beams. The latter are obtained by fitting the free parameters v_0 and α of the function

$$n(v) = \text{const}\ v^2 \exp\{-[(v - v_0)/\alpha]^2\} \qquad (1)$$

to the TOF profiles. The analysis of the scattering data requires a precise knowledge of the absolute velocities. It is achieved by measuring TOF profiles for two positions of the chopper wheel separated by a well-known distance. The technique eliminates uncertainties in the residence times of the ions within the detectors and in the starting time of a beam pulse. The (estimated) error for the absolute velocity is below 0.5%. Important dimensions, the beam operating conditions and the resulting velocity parameters, are compiled in Table 1.

The product molecules KI and the elastically (nonreactively) scattered K atoms are detected with nearly equal probability by surface ionization on a Re ribbon located 49 cm away from the intersection volume. The ribbon is housed in a separately pumped ultrahigh vacuum chamber which can be rotated around the scattering volume in the plane of the two beams (scattering plane). The ions desorbing from the Re ribbon are accelerated to a channeltron and converted to electron pulses which are subsequently amplified, discriminated, shaped, and eventually counted. For phase sensitive counting the iodobenzene beam is chopped at a frequency of 15 Hz. The velocity distributions of scattered particles have been determined with the aid of a conventional TOF analyzer which employs a path length of 42 cm. The pulses are routed to a pair of scalers or a forward−backward counting multichannel analyzer both synchronized to the beam chopper depending on whether an angular distribution or a TOF profile of the scattered particles is measured.

TABLE 2: Molecular Constants for C_6H_5I and Brute Force Parameters

		ref
rotational constants (cm^{-1})		
A_0	0.18917	30
B_0	0.02503	30
C_0	0.02210	30
dipole moments (D)		
$d = d_a$	1.70	31
$d_b = d_c$	0	
C−I bond		
D_0 (eV)	2.7 ± 0.1	32
R_m (Å)	2.08	33
ω_0 (cm^{-1})	270	34
brute force parameters		
$\|\mathcal{E}\|$ (kV/cm)	20	
$\bar{\omega}$	24.2	35
A_0	0.025	

The C_6H_5I molecules are oriented by means of the brute force technique.[1] The field electrodes are two parallel plates 1 cm apart, which stand perpendicular to the scattering plane. The intersection volume is located in the center of the space between the plates. A slit through the plates along the scattering plane allows the beams and scattered particles to pass freely. Voltages of opposite sign are applied to the plates to create the orientation field; with ±12.5 kV we achieve a field strength of 20 kV/cm at the reaction volume. The field vector lies parallel to the scattering plane and can be rotated by rotating the electrodes. The field direction is reversed by an interchange of the voltage polarity.

The C_6H_5I molecule is an asymmetric rotor of the C_{2v} point group. It possesses an electric dipole moment **d** which is directed along the C_2 symmetry axis from I to C. A few molecular constants are compiled in Table 2. In this paper we define the direction of the symmetry axis **â** by the inverse direction of the dipole moment

$$\hat{\mathbf{a}} = -\hat{\mathbf{d}} \qquad (2)$$

The interaction of the dipole with the electric field leads to a net orientation of the molecular axis, that is, to an anisotropic directional distribution of the axis which features a preferred direction. Formally, this distribution is described by a probability density function $\tilde{A}(\cos\theta)$ where θ is the angle between the orientation field $\mathcal{E}$ and the figure axis **â**. The probability to find the axis pointing into the solid angle dω is given by

$$dw = \tilde{A}\,(\cos\theta)\,d\omega \qquad (3)$$

where $\tilde{A}$ is normalized according to $\int\tilde{A}(\cos\theta)\,d\omega = 1$.

The problem of calculating the axis distribution of an asymmetric top molecule has been attacked only recently and is described in detail elsewhere.[22] The applied computational method is a generalization of the one used for linear and symmetric top molecules.[2a,11b,23] It requires as input the population of rotational states of the reagent molecules upstream from the orientation field in the field free region. The calculations for C_6H_5I based on a Boltzmann distribution with rotational temperature T_{rot} provide

$$\tilde{A}(\cos\theta) = \frac{1}{4\pi}(1 - A_0 \cos\theta) \qquad (4a)$$

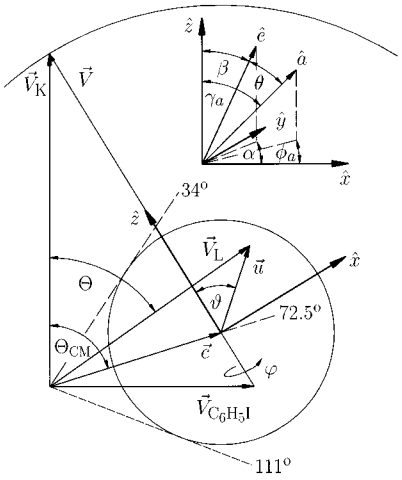

Figure 1. Newton diagram for R1 drawn for the mean beam velocities. Illustrated is the relation between the velocity u and scattering angle ϑ of the detected product in the CM frame $\hat{\mathbf{x}}$, $\hat{\mathbf{y}}$, $\hat{\mathbf{z}}$ and the corresponding quantities V_L, Θ in the LAB frame. The insert defines the polar angle of the orientation field $\boldsymbol{\mathcal{E}} = \hat{\mathbf{e}}|\boldsymbol{\mathcal{E}}|$ and the molecular symmetry axis $\hat{\mathbf{a}}$ in the CM frame. Further details are given in the text.

with

$$A_0 = 0.0386 \frac{|\boldsymbol{\mathcal{E}}|(\mathrm{kV/cm})}{T_{\mathrm{rot}}(K)} \qquad (4b)$$

For further applications (section IV.A) it is useful to replace $\cos\theta$ by quantities defined in the center-of-mass frame (see Figure 1) and one obtains

$$\tilde{A}(\cos\theta) = \frac{1}{4\pi}\{1 - A_0[\cos\gamma_a \cos\beta + \sin\gamma_a \sin\beta \cos(\phi_a - \alpha)]\} \quad (5)$$

where γ_a, ϕ_a, and β, α are the polar angles of the molecular symmetry axis $\hat{\mathbf{a}}$ and of the electric field $\boldsymbol{\mathcal{E}} = \hat{\mathbf{e}}|\boldsymbol{\mathcal{E}}|$.

A rough estimate for T_{rot} is the translational temperature $T_{\parallel}$ of the nozzle beam extracted from the width parameter α of eq 1; we find $T_{\parallel} = 148$ K (Table 1) and obtain for the standard field strength of 20 kV/cm $A_0 = 0.0042$. In an attempt to gain more direct information about the state distributions, we have performed a beam deflection experiment[24] similar to those performed by Herschbach and co-workers in the 1960s.[25] A preliminary analysis of the data suggests an approximate temperature of $T_{\mathrm{rot}} \approx 31$ K, and one obtains for 20 kV/cm the value $A_0 = 0.025$; it agrees with the lower boundary deduced from the observed steric effects (see section V).

III. Experimental Results

A. Scattering from Nonoriented Molecules. The experiments have been performed at a mean collision energy of $E_{\mathrm{tr}} = 1.9$ eV. The kinematic situation is illustrated by the Newton diagram Figure 1 drawn for the mean beam velocities. The tip of the center-of-mass velocity vector **C** defines the origin of the (Cartesian) CM frame $\hat{\mathbf{x}}$, $\hat{\mathbf{y}}$, and $\hat{\mathbf{z}}$ where $\hat{\mathbf{z}}$ is parallel to the relative velocity **V** and the $\hat{\mathbf{x}}$, $\hat{\mathbf{z}}$ plane is parallel to the plane of the beam velocities. The polar coordinates ϑ,φ of the velocity **u** of the detected product (KI) are the scattering angles in the CM frame; $\mathbf{V_L}$ and Θ denote the product velocity and scattering angle in the laboratory (LAB) frame. The radii of the outer and inner circles around the tip of the vector **C** correspond to the velocity of elastically scattered K atoms and the maximal recoil velocity of the product KI allowed by energy conservation, respectively. Accordingly, products can be observed only between $\Theta = 34°$ and 111°. At smaller and larger angles the signal is due to elastically (nonreactively) scattered K atoms only. Between the boundaries both processes contribute; the scattered particles K and KI are detected irrespective of their nature but can be distinguished by their substantially different velocities.

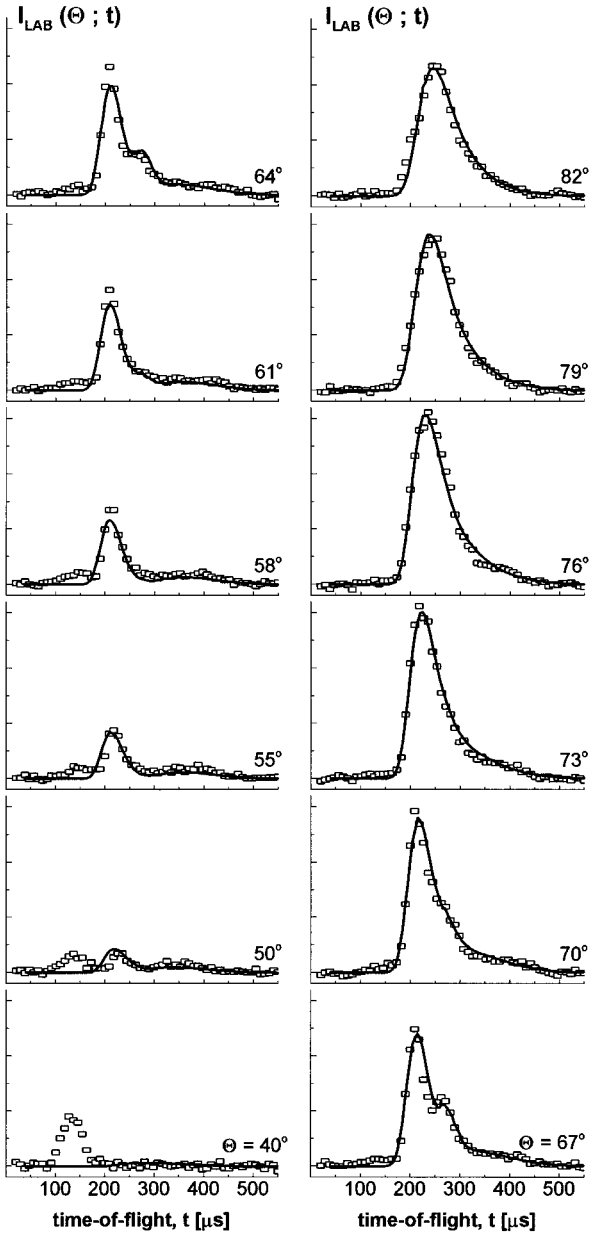

Figure 2. Time-of-flight distributions of scattered particles measured at the indicated laboratory scattering angles Θ. The structure at small t is due to elastically (nonreactively) scattered K atoms. The main peak results from reactively scattered KI. Note the additional structure in the descending slope of the peak between 61° and 70°. The solid lines are best fit simulations of the reactive section of the TOF profiles.

A sample of TOF profiles $I_{\mathrm{LAB}}(\Theta;t)$ measured at various scattering angles is presented in Figure 2. At $\Theta = 40°$ only one peak appears at small time-of-flights which is attributed to elastically scattered K atoms (see Newton diagram Figure 1). At 50° a second well-resolved peak emerges at larger times which is associated with the flux of KI. With increasing angle the reactive peak gains intensity while the elastic intensity decreases and eventually vanishes. Between 61° and 70° another structure appears in the descending slope of the reactive peak which forms even a marginally resolved peak at 64° and 67°. The nature of the process creating this structure is not yet clear; it appears most likely at present that again KI is formed

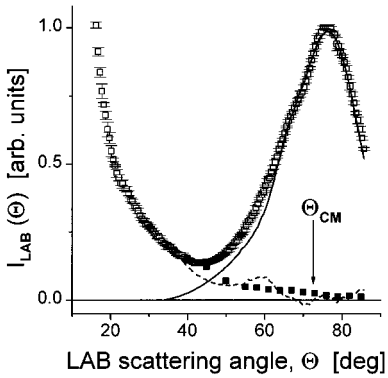

Figure 3. Angular distribution of scattered particles. The steep descent at small angles is due to elastically (nonreactively) scattered K atoms and the main peak results from reactively scattered KI. The solid squares represent the intensity of the scattered K atoms in the overlap region which has been isolated from the total intensity using the TOF profiles. The dashed and solid lines are best fit simulations of the nonreactive and reactive scattering intensity, respectively.

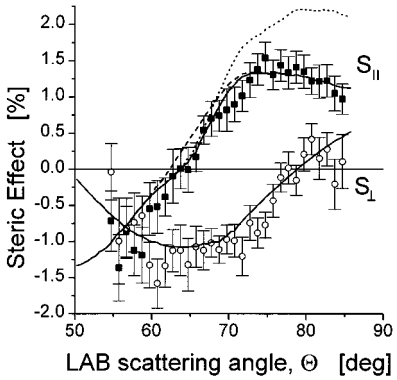

Figure 4. Parallel (■) and perpendicular (○) steric effect. The solid lines are best fit simulations. The dashed line is the result of a simulation where the minor component is ignored. The dotted line is the prediction of the DIPR model.

but by a different mechanism. Other processes and products cannot be excluded as yet and are discussed at the end of section V. The solid lines in Figure 2 are results of the data analysis. The curves simulate well the features of the dominant KI component and of the minor one; the peaks due to elastic scattering are not included in the simulation.

The angular distribution of the (velocity integrated) flux of scattered particles $I_{LAB}(\Theta)$ is shown in Figure 3. The steep descent at small scattering angles outside the boundary of products is typical for elastic scattering. Within the boundaries the intensity reaches near 43° a minimum and starts rising with growing angle due to the onset of product flux. The product intensity then forms a peak at 74° slightly shifted with respect to the centroid angle $\Theta_{CM} = 72.5°$. In the overlap region the purely elastic (nonreactive) and reactive contributions can be separated using the ratio of counts accumulated in the elastic and product domain of the TOF profiles. The resulting elastic scattering intensity is given by the solid squares in Figure 3. Beginning at small angles, it continues the initial decline smoothly and vanishes beyond 70°. The solid and dashed lines in Figure 3 represent the best fit simulation of the pure reactive and the simulation of the pure elastic portion of the total intensity, respectively, where the latter is the difference between measured intensity and the solid curve. The data points are well recovered; minor deviations occur only near the onset of product flux.

B. Orientation Effects. The reagent molecules have been oriented as described in section II. Two data sets were measured each consisting of two angular distributions of products measured for different directions of the orientation field $\mathcal{E}$. For one set the field directions were chosen parallel and antiparallel to the mean relative velocity **V**. From the corresponding angular distributions $I^{||}_{LAB+}(\Theta)$ and $I^{||}_{LAB-}(\Theta)$ the parallel steric effect defined by

$$S_{||}(\Theta) = \frac{I^{||}_{LAB+}(\Theta) - I^{||}_{LAB-}(\Theta)}{I^{||}_{LAB+}(\Theta) + I^{||}_{LAB-}(\Theta)} \tag{6}$$

has been determined. For the other set the directions of $\mathcal{E}$ were chosen perpendicular to **V** pointing toward and away from the detector. The corresponding angular distributions were then used to calculate the perpendicular steric effect according to

$$S_{\perp}(\Theta) = \frac{I^{\perp}_{LAB+}(\Theta) - I^{\perp}_{LAB-}(\Theta)}{I^{\perp}_{LAB+}(\Theta) + I^{\perp}_{LAB-}(\Theta)} \tag{7}$$

To minimize errors resulting from intensity drifts of the beams the steric effects are measured individually for each angle Θ. For this purpose the signal is measured for a period of 60 s for a given direction of $\mathcal{E}$, then the field is reversed and the signal is measured again for the same period. This is continued until the error of the difference of intensities reaches a preselected margin.

The results are shown in Figure 4. The two steric effects feature markedly different shapes with extremal values of nearly 1.5% (3% of the signal intensity). $S_{||}(\Theta)$ starts negative at smaller angles and rises with Θ. It assumes a zero near 64° and a peak at around 76° close to the maximal product flux. Subsequent to the peak $S_{||}(\Theta)$ declines slowly. The positive sign indicates that wherever $S_{||} > 0$ more products are detected if the electric field is parallel to **V** than for the opposite direction. Since the sign is positive over the entire range of significant product intensity, the result suggests that KI is favorably formed if the K atoms attack the I end of iodobenzene. At smaller angles just the opposite is the case, however this concerns only a small fraction of product flux. $S_{\perp}(\Theta)$ exhibits a sinusoidal shape with a negative minimum near 64° and a zero around 78°, near the angle of peak product intensity. The existence of a nonvanishing perpendicular steric effect is a clear manifestation of a correlation between the direction of the molecular axis and of the product flux. If both directions would be uncorrelated, $S_{\perp}(\Theta)$ would vanish. The negative sign indicates that wherever $S_{\perp} < 0$ more products are scattered into the direction of the molecular axis than into the opposite one. The lines through the data points refer to simulations and model calculations discussed in section V.

IV. Data Analysis

A. Observed Quantities. To analyze the data, we follow closely the procedures presented in detail previously[1−3] and introduce the fundamental orientation-dependent double-differential reaction cross section $I(\cos\gamma_a, \phi_a, \vartheta, \varphi, u)$ in the CM frame. The observable double-differential reaction cross section $J_{\hat{e}}(\vartheta,\varphi,u)$ is then an average over the prepared axis distribution (eq 5).

$$J_{\hat{e}}(\vartheta,\varphi,u) = \int_{4\pi} I(\cos\gamma_a, \phi_a, \vartheta, \varphi, u)\tilde{A}(\cos\gamma_a, \phi_a)\, \mathrm{d}\cos\gamma_a\, \mathrm{d}\phi_a \tag{8}$$

To quantify the extent of information on $I(\cos\gamma_a, \phi_a, \vartheta, \varphi, u)$ not canceled by the averaging procedure we expand the cross section

in a series of real spherical harmonics

$$I(\cos\gamma_a, \phi_a, \vartheta, \varphi, u) = \sum_{l=0}^{\infty}\sum_{m=0}^{l} J_{lm}(\vartheta,u)\cos[m(\varphi-\phi_a)]P_l^m(\cos\gamma_a) \quad (9)$$

and insert the expansion together with $\tilde{A}(\cos\gamma_a, \phi_a)$ from eq 5 into eq 8. Thanks to the linear dependence of $\tilde{A}$ on $\cos\gamma_a$ and $\sin\gamma_a$ and the well-known orthogonality relations only three terms of the infinite sum survive

$$J_{\hat{e}}(\vartheta,\varphi,u) = J_{00}(\vartheta,u) - A_0{}^1/_3[J_{10}(\vartheta,u)\cos\beta + J_{11}(\vartheta,u)\cos(\varphi-\alpha)\sin\beta] \quad (10)$$

The three accessible moments are given by the fundamental cross section via

$$J_{00}(\vartheta,u) = \frac{1}{4\pi}\int I(\cos\gamma_a, \phi_a, \vartheta, \varphi, u)\, \mathrm{d}\cos\gamma_a\, \mathrm{d}\phi_a \quad (11a)$$

$$J_{10}(\vartheta,u) = \frac{3}{4\pi}\int I(\cos\gamma_a, \phi_a, \vartheta, \varphi, u)\cos\gamma_a\, \mathrm{d}\cos\gamma_a\, \mathrm{d}\phi_a \quad (11b)$$

$$J_{11}(\vartheta,u) = \frac{3}{4\pi}\int I(\cos\gamma_a, \phi_a, \vartheta, \varphi, u)\sin\gamma_a \times \cos(\varphi-\phi_a)\, \mathrm{d}\cos\gamma_a\, \mathrm{d}\phi_a \quad (11c)$$

where J_{00} is the average of the cross section over all orientations. This is the usual double-differential reaction cross section observable in experiments with randomly oriented molecules. The two other moments are weighted averages probing different domains of the fundamental cross section. They are the leading terms of the orientation dependence of the reactive process and provide additional information on the dynamics.

The relation between the observable quantity $J_{\hat{e}}(\vartheta,u)$ and the measured TOF profiles is formally given by

$$I_{\mathrm{LAB},\hat{e}}(\Theta,t) = \mathrm{const}\,\langle J^{\Sigma}_{\hat{e}}(\vartheta,u)\rangle \quad (12)$$

where the bracket $\langle ...\rangle$ denotes transformation of the CM variables to the LAB frame (see Figure 1), averaging over the beam velocity profiles and an integration over the shutter function of the TOF analyzer; for more details see ref 1. The upper index of $J^{\Sigma}_{\hat{e}}$ has been included to symbolize that several components might contribute to the detected flux of scattered particles. Using eqs 6, 7, 10, and 12 one obtains for the three experimental conditions: (i) orientation field turned off ($A_0 = 0$), (ii) orientation field on and parallel/antiparallel to **V** ($\beta = 0°$ *and* 180°) and (iii) two opposite directions perpendicular to **V** ($\beta = 90°$, $\alpha = 0°$, and 180°) the measured quantities: (i) TOF profiles

$$I_{\mathrm{LAB}}(\Theta,t) = \mathrm{const}\,\langle J^{\Sigma}{}_{00}(\vartheta,u)\rangle \quad (13)$$

(ii) parallel steric effect

$$S_{\|}(\Theta) = -\frac{1}{3}A_0\frac{\langle\langle J^{\Sigma}_{10}(\vartheta,u)\rangle\rangle V_{\mathrm{L}}}{\langle\langle J^{\Sigma}_{00}(\vartheta,u)\rangle\rangle V_{\mathrm{L}}} \quad (14)$$

(iii) perpendicular steric effect

$$S_{\perp}(\Theta) = -\frac{1}{3}A_0\frac{\langle\langle J^{\Sigma}_{11}(\vartheta,u)\cos\varphi\rangle\rangle V_{\mathrm{L}}}{\langle\langle J^{\Sigma}_{00}(\vartheta,u)\rangle\rangle V_{\mathrm{L}}} \quad (15)$$

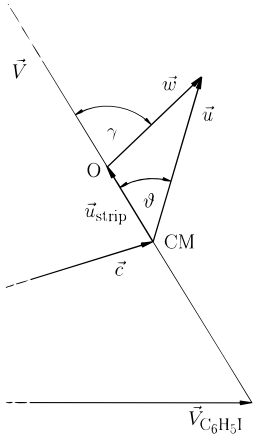

Figure 5. Section of the Newton diagram illustrating the relation between scattering angle γ and product velocity **w** in the O-frame and the corresponding quantities ϑ, u in the CM frame. $\mathbf{u}_{\mathrm{strip}}$ is the spectator stripping velocity of KI products defined by eq 16.

where the outer brackets $\langle ...\rangle$ indicate integration over the product velocity (or time-of-flight).

B. Determination of the Moments by a Least-Squares Fit Procedure. *1. The Coordinate Frame.* In the following the three moments will be extracted from the three data sets: (a) the section of the TOF profiles $I_{\mathrm{LAB}}(\Theta,t)$ attributed to reactive scattering, (b) $S_{\|}(\Theta)$, and (c) $S_{\perp}(\Theta)$, using the least-squares fit technique. First, parameterized trial functions for the moments are inserted into eqs 13−15, then the measured quantities are simulated by performing the computations prescribed by the brackets, and finally, the parameters are varied until the simulated and measured data agree best in the least-squares sense. The quality of the resulting fit depends on the analytic form of the chosen trial functions but also on the coordinate system used for the description of the scattering. We resort to a frame whose axes are parallel to the usual CM frame but whose origin moves relative to the latter with a constant velocity (O-frame). This velocity is, in principle, free and can be adjusted to the considered problem. We set it to the spectator stripping velocity of KI

$$\mathbf{u}_{\mathrm{strip}} = \frac{M_{\mathrm{K}}M_{C_6H_5}}{M_{\mathrm{KI}}M}\mathbf{V} \quad (16)$$

where the M_i denote the masses of the indicated particles and M is the total mass. The mass factor amounts to 0.074. $\mathbf{u}_{\mathrm{strip}}$ results as product velocity in the CM frame in case the nonreacting constituent of the reagent molecule plays only the role of a spectator. As shown below, this choice for the relative velocity of the frames will simplify both the analysis of the data and the interpretation of the results. The relation between the scattering angle γ and recoil velocity **w** in the O-frame and the corresponding quantities in the CM frame are illustrated by Figure 5; analytic expressions are given in Appendix 1 (see also ref 3a). The double-differential reaction cross sections in the two frames are related by

$$J_{\hat{e}}(\vartheta,u) = \left(\frac{u}{w}\right)^2 J_{\hat{e}}(\gamma,w) \quad (17)$$

where $(u/w)^2$ is the Jacobian of the transformation; the moments are transformed accordingly.

2. The Moment J_{00}. To simulate the reactive section of the TOF profiles we ignore the elastic contribution in eq 13 and

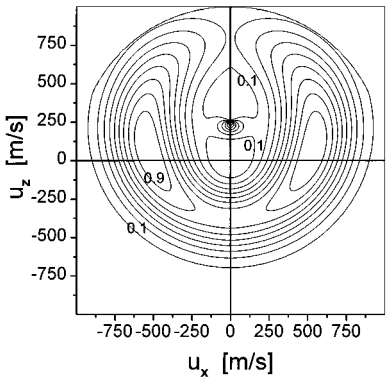

Figure 6. Polar diagram of the double-differential reaction cross section in the CM frame for the scattering from randomly oriented molecules. The contour map represents the best fit trial functions. Length and angle of the radius vector with the *z*-axis are equal to u and ϑ. Note the preferred sideways scattering and the narrow peak in the center.

choose an ansatz for the trial function in the O-frame which contains two terms

$$J_{00}^{\Sigma}(\gamma,w) = J_{00}(\gamma,w) + J_{00}^{m}(\gamma,w) \tag{18}$$

where the first one describes the gross features caused by the dominant KI component and the second one takes care of the minor component causing the secondary structure in the descending slope of the TOF profiles ($61° \leq \Theta \leq 70°$). For both components the cross section in the O-frame is assumed to be separable into a product of an angle and a velocity dependent factor

$$J_{00}(\gamma,w) = G(\gamma)W(w) \tag{19a}$$

$$J_{00}^{m}(\gamma,w) = G^{m}(\gamma)\, W^{m}(w) \tag{19b}$$

The analytic form of the various trial functions employed are given in Appendix 2 together with the best fit parameters. The best fit simulations are shown in Figures 2 and 3 as solid lines. The TOF profiles including the secondary structure are well recovered; good agreement with the angular distribution of product intensity (after substraction of the elastic contribution) is also achieved.

The best fit trial functions are displayed in Figure 6 as a contour map. Plotted as polar diagram is the sum of the two terms of eq 18 properly transformed into the CM frame;[26] length and angle with the z-axis of the radius vector are equal to the product velocity $|\mathbf{u}|$ and the scattering angle ϑ, respectively. The two contributions are well separated: the minor component J_{00}^{m} is localized near the center of the contour map, while the dominant KI component J_{00} covers most of the plot. Integration of the two terms over u and solid angle furnishes a branching ratio of the integral cross sections of $\sigma^m/\sigma = 0.65\%$. The most prominent features of the contour map are the following: J_{00} exhibits preferred sideways scattering with peak intensity near $\vartheta = 75°$ at a velocity amounting to 60% of the maximal one; J_{00}^{m} is sharply forward peaked and appears close to the stripping velocity with an extremely small velocity spread.

The angular and velocity distributions of the dominant KI component are shown in the upper panel of Figure 7. The angular distribution has been determined by integrating $J_{00}(\vartheta,u)$ (see contour map) over u. The preferred sideways scattering with peak intensity at 75° is clearly visible. A sample of product velocity distributions determined for various scattering angles is displayed in Figure 7b. The curves do depend on the scattering angle significantly. As a consequence, any attempt to analyze the TOF profiles with the aid of the usual product ansatz in the CM frame would provide fits of minor quality.

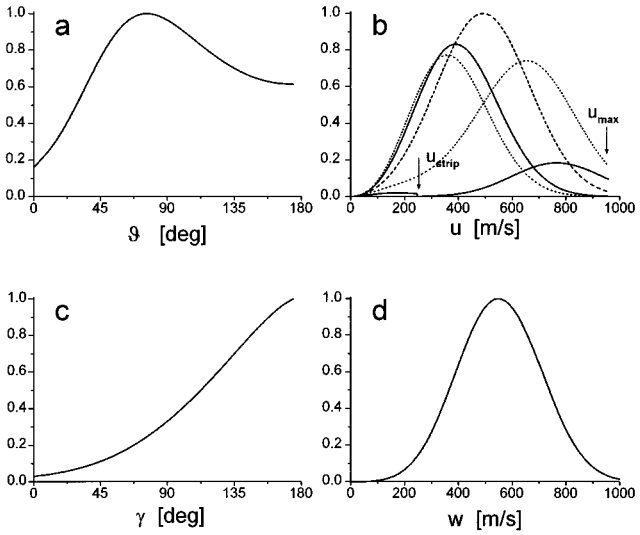

Figure 7. Upper panel: Angular and velocity distributions of the dominant KI component in the CM frame deduced from the best fit trial functions: (a) angular distribution, (b) velocity distributions at the angles $\vartheta = 0°$ (right solid line), 45° (right dotted line), 90° (central dashed line), 135° (left solid line), 180° (left dotted line). Lower panel: same as in the upper panel but in the O-frame: (c) $G(\gamma)$, (d) $W(w)$. u_{strip} is the spectator stripping velocity of KI products defined by eq 16; u_{max} is the mean maximal recoil velocity of KI.

TABLE 3: Energetics

	E_{tr}	ΔD	E_{tot}	$\overline{E'_{tr}}/E_{tot}$	$\overline{E'_{int}}/E_{tot}$
dominant KI	1.90	0.6	2.5	31.5%	68.5%
minor KI	1.90	0.6	2.5	5.3%	94.7%

One would be forced to abandon the simple ansatz and use ϑ dependent velocity distributions which require more complicated functions and additional parameters. Thus one important benefit of the O-frame is that these complications can be avoided. The angle averaged product mean translational energy amounts to $E_{tr} = 31.5\%$ of the totally available energy. The remainder of 68.5% is vested in the internal energy of the product molecules KI and C_6H_5. The energetics are compiled in Table 3.

The corresponding distributions of KI in the O-frame are displayed in the lower panel of Figure 7. Very surprisingly, $G(\gamma)$ (Figure 7c) exhibits, contrary to the angular distribution in the CM frame (Figure 7a), a sharp peak in the backward direction followed by a continuous descent to 1/28 of the peak intensity at $\gamma = 0°$. An inspection of the transformation procedure shows, that this difference is a trivial consequence of the Jacobian of the O $\leftrightarrow$ CM frame transformation. Intensity scattered into the backward direction of the O-frame, say around the most probable velocity, is suppressed in the CM frame due to the resulting small velocities u. With decreasing γ u grows and the Jacobian overcompensates the decay of the intensity until the peak intensity in the CM frame is reached beyond which the drastic decay of $G(\gamma)$ dominates and causes the steep slope. The velocity distribution $W(w)$ is by definition (eq 19b) independent of γ.

The angular and velocity distributions in the CM frame of the minor component are illustrated in the upper panel of Figure 8. The findings are unusal in any respect: the angular distribution (Figure 8a) indicates extremely sharp forward scattering; the velocity distribution (at $\vartheta = 0°$) (Figure 8b) is very narrow and assumes a maximum near the stripping velocity (250 m/s). Assuming KI as minor product the angle averaged, mean translational energy amounts only to $E_{tr} = 5.3\%$ of the totally available energy; consequently, the products have absorbed 94.7% (Table 3). The corresponding distibutions in the O-frame are shown in the lower panel of Figure 8. $G^m(\gamma)$

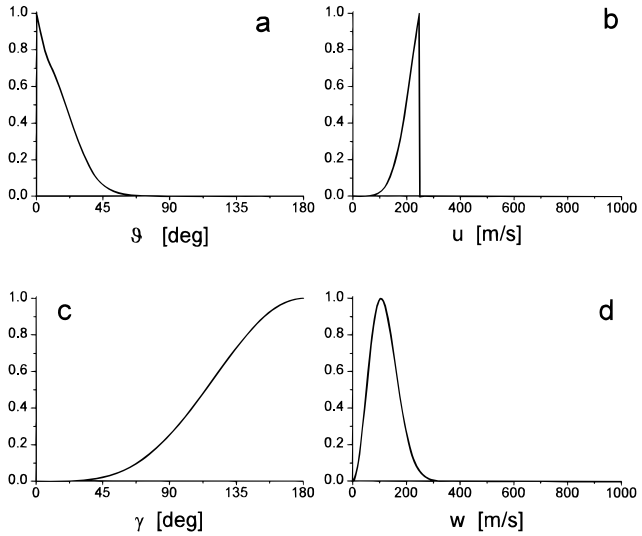

Figure 8. Same as in Figure 7 but for the minor component.

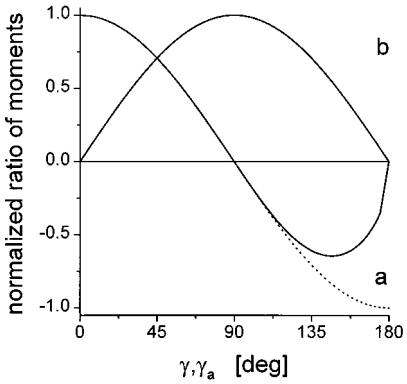

Figure 9. Ratio of moments in the O-frame for the dominant KI component. (a) $J_{10}/(3a_{10}\,J_{10})$, the solid line is the result of the best fit simulation of the parallel steric effect. The dashed line is the prediction of the DIPR model, it coincides with the trial function at angles ≤90°. (b) $J_{11}/(3a_{11}\,J_{00})$, the curve is obtained from the simulation of the perpendicular steric effect. It coincides completely with predictions of the DIPR model (not shown).

(Figure 8c) indicates preferred scattering intensity into the backward direction again in contrast to the results in the CM frame (Figure 8a). The different appearance in the CM frame is due to the fact that the width of the velocity distribution $W^m(w)$ (Figure 8d) is significantly smaller than the stripping velocity. Thus the intensity scattered at any angle in the O-frame appears in the CM frame close to the forward direction.

3. The Moments J_{10} and J_{11}. For the determination of the moments J_{10} and J_{11}, only the velocity integrated data $S_{\parallel}(\Theta)$ and $S_{\perp}(\Theta)$ are available which contain only limited information particularly about the u dependence of the moments and on the various components contributing to eqs 14 and 15. We assume that elastic scattering exhibits no significant steric effect and ignore this component in the nominator of eqs 14 and 15. The denominator is proportional to the total scattering intensity and the elastic portion is included. First, we concentrate on the dominant KI component.

The ansatz for the trial functions is suggested by the correlation between the orientation of $\hat{\mathbf{a}}$ and the direction of the product flux implied by the nonvanishing $S_{\perp}$. We assume that $I(\cos\gamma_a, \phi_a, \vartheta, \varphi, u)$ is essentially nonzero only in a domain centered around $\gamma_a \approx \vartheta$ and $\phi_a \approx \varphi$. An approximate evaluation of the integrals eqs 11a−c then provides $J_{10} \approx 3J_{00}\cos\vartheta$ and $J_{10} \approx 3J_{00}\sin\vartheta$. We make these results somewhat more flexible and extend them to the O-frame by defining the following trial functions

$$J_{10}(\gamma,w) = 3a_{10}\,J_{00}(\gamma,w)\,f_{10}(\gamma)\cos\gamma \qquad (20)$$

$$J_{11}(\gamma,w) = 3a_{11}\,J_{00}(\gamma,w)\,f_{11}(\gamma)\sin\gamma \qquad (21)$$

where f_{10} and f_{11} are simple functions subject to the condition $0 \le f_{10}, f_{11} \le 1$ which accommodate the parameters; regarding the limited information of the data we include only an angular dependence. a_{10} and a_{11} are adjustable constants. The analytic form of the trial functions and best fit parameters are given in Appendix 2.

First we consider simulations of the parallel steric effect. The dashed line in Figure 4 is the best fit simulation calculated with the assumption that only the dominant KI component contributes to the steric effect and the minor component can be ignored. The simulation recovers most of the data but a slight departure remains near the zero up to $\Theta = 70°$, exactly in the region where the minor component provides intensity. This suggests consideration also of the minor component. Due to limited information we assume that the minor component features the moment $J^m_{10} = -3J^m_{00}\cos\gamma$ and use $J^{\Sigma}_{10} = J_{10} + J^m_{10}$. The result of the computation is given by the solid line in Figure 4; the curve recovers now the data nearly perfectly over the entire range. If a positive sign is used for the minor component, the simulation deteriorates and within the corresponding region deviations occur far outside the error bars.

The perpendicular steric effect is not sensitively dependent on the presence of a contribution from the minor component since this product flux appears in the CM frame only in close vicinity to the relative velocity. Due to the cos φ term in eq 15 the integrand changes sign when the integration variable V_L crosses this area and the integral vanishes practically. A good fit of the data (solid line in Figure 4) is obtained for $f_{11} \equiv 1$. A reduction of the moment near $\gamma = 180°$ as required for the parallel effect leads only to insignificant modifications for a similar reason as discussed above. The ratio of moments for the dominant KI component (a) $J_{10}/(3a_{10}\,J_{00})$ and (b) $J_{11}/(3a_{11}\,J_{00})$ are depicted in Figure 9; (a) follows cos γ up to 120° where significant deviations start developing while (b) is purly sinusoidal.

The constants a_{10} and a_{11} result from the absolute value of the steric effects, which is proportional to the orientation parameter A_0. The simulation procedure provides $A_0\,a_{10} = 0.025$ and $A_0\,a_{11} = 0.025$; isolation of the amplitudes thus requires the exact knowledge of A_0. Using the most probable value $A_0 = 0.025$, we obtain $a_{10} = a_{11} = 1$.

V. Discussion

The observed steric effects and the extracted moments are clear evidence for the existence of a tight correlation between the orientation of the molecular axis $\hat{\mathbf{a}}$ and the direction of the product flux characterized by $\vec{\mathbf{u}}$. A simple rationale for such a correlation provides the DIPR model. We start with a brief discussion of the model and compare thereafter the predictions with the data. More details and the derivation of analytic expressions for the moments are given elsewhere.[1−3]

The basic assumptions of the model for R1 are (i) K and C_6H_5I approach eachother on straight trajectories (ii) at a critical distance the reaction is suddenly initialized by a rapid dissociation (explosion) of the I−C bond along the symmetry axis, (iii) the phenyl radical C_6H_5 leaves the scene without interaction with K and I. The recoil velocity of C_6H_5 in the CM frame is then the sum of the initial velocity of C_6H_5I and the velocity gained during the explosion (internal motion is neglected). Conservation of momentum provides then for the velocity of

KI in the CM frame the basic relation

$$\mathbf{u} = \mathbf{u}_{\text{strip}} + \mathbf{w} \tag{22}$$

where $\mathbf{u}_{\text{strip}}$ is defined by eq 16.

The product velocity **u** is thus composed of a trivial constant and a dynamically important component, $\mathbf{u}_{\text{strip}}$ and **w**, respectively. The latter characterizes the explosion of the C−I bond and determines the dynamics of the process. Therefore, it appears suitable to eliminate the constant velocity by a coordinate transformation and describe the scattering in terms of **w** rather than **u**. As a benefit one may expect that the differential cross section formulated in the new frame will be free of any obscuring additions caused by the constant velocity and reflect only the essential dynamics of the process. The new frame is identical to the O-frame introduced before (Figure 5).

R1 is an illustrative example for a beneficial use of the O-frame. We found that the differential cross section in the O-frame is separable into two simple functions but after the transformation into the usual CM frame the separability is lost and an analytic description would be very involved. In the light of the above statement this result is an indication for the presence of an impulsive mechanism. In addition, we conclude that the preferred backward scattering in the O-frame reflects the dynamics of R1 rather than the preferred sideways scattering in the CM frame. The presentation in the O-frame thus reveals that the mechanism of R1 is akin to the one of $K + CH_3I$ rather than to the mechanisms suggested for the sideways reactions $M + CCl_4$,[27] $Cs + CH_3I$,[28] and $K + CH_3Br$.[4] Moreover, at least for the latter two reactions, the O ↔ CM transformation could provide an alternative rationale for the observed sideways scattering.

To allow predictions for steric effects, the list of assumptions must be extended by an entry about the relative directions of the molecular axis prior to collision **â** and at the instant when the C−I bond explodes. We neglect any reorientation of the symmetry axis during the approach and assume that the fragments separate along the initial direction of the axis. In the O-frame the KI products move then parallel to **â** with the velocity

$$\mathbf{w} = \sqrt{2R\,\frac{M_{C_6H_5}}{M_{KI}M}}\,\hat{\mathbf{a}} \tag{23}$$

where the M_X denote the masses of the indicated particle, M is the total mass. The magnitude of **w** is determined by the energy R released during explosion. The scattering angles in the O-frame are then dictated by the initial orientation of the molecule and thus

$$\gamma \equiv \gamma_a; \quad \varphi \equiv \phi_a \tag{24}$$

hold. A direct consequence of the tight **â**, **w** correlation (eq 23) is the analytic form of the predicted moments

$$J_{10} = 3J_{00} \cos \gamma_a \tag{25}$$

$$J_{11} = 3J_{00} \sin \gamma_a \tag{26}$$

These functions are very similar to the ansatz we used before, except that all prefactors and correction functions are unity and the scattering angle γ is replaced by the angle of attack γ_a.

A comparison of these predictions with our least squares fit results is displayed in Figure 9. Equation 26 recovers the purely sinusoidal shape of the best fit ratio of moments $J_{11}/(3a_{11}\,J_{00})$ over the entire angular range (solid line b). The curve for $J_{10}/(3a_{10}\,J_{00})$ obtained from eq 25 (dashed line a) is congruent with the best fit ratio over an extended interval up to around $\gamma = 135°$. But toward larger angles in the domain of backward scattering significant deviations occur. Of course, considering the simplicity of the model and the complexity of the system, deviations from the model must be expected. On the other hand, the observed departures might be even more moderate than they look like on the first glance. It cannot be excluded that highly inelastic processes contribute intensity to the total signal, particularly at large scattering angles, which is undistinguishable from the product flux. This mimics steric effects smaller than the one expected for pure reactive scattering. If corrected for, the modifications of the moment would be less marked and f_{10} may even become unity.

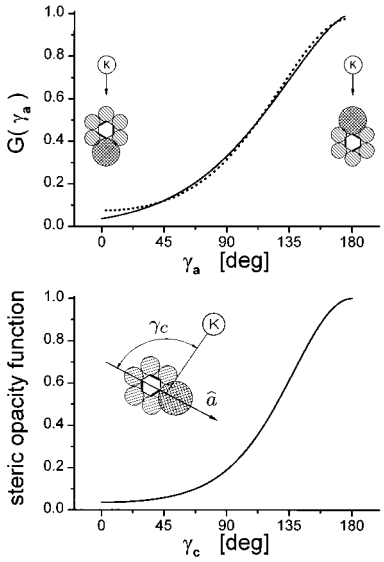

Figure 10. Upper panel: orientation dependent integral reaction cross section for the dominant KI component versus the angle of attack γ_a. KI is favorably formed if K attacks the I end of iodobenzene (head); the reaction is almost completely hindered if K approaches the C_6H_5 end (tail). The dashed line is a simulation based on the steric opacity function shown in the lower panel. Lower panel: Steric opacity function versus the C_6H_5−I−K bond angle of the transition state. The half-width of the curve defines an apex angle of the cone-of-acceptance of ≈110°.

Somewhat problematic are the absolute values of the experimentally determined moments due to the uncertainties of the orientation parameter A_0. Perfect agreement with the DIPR predictions $a_{10} = a_{11} = 1$ is obtained for the most probable value $A_0 = 0.025$ (see section IV.B.3). The definitions of the moments eqs 11a−c supply the upper boundaries for the ratios $J_{10}/3J_{00} \leq 1$ and $J_{11}/3J_{00} \leq 1$. Insertion of the upper limit into eqs 20 and 21 provides then a_{10}, $a_{11} \leq 1$. The experimental result $A_0\,a_{10} = 0.025$ eventually leads to the lower limit $A_0 \geq 0.025$. Consequently, the value $A_0 = 0.0042$ derived in Section II is inconsistent with the size of the steric effects. An upper boundary for T_{rot} follows if the smallest value $A_0 = 0.025$ is inserted into eq 4b. With $|\mathcal{E}| = 20$ kV/cm one obtains $T_{\text{rot}} \leq 31$ K. A significantly smaller temperature is in contradiction with the deflection experiments and considered unlikely. In summary we conclude that, in addition to the shapes, the DIPR model recovers also the absolute values of the moments.

Within the DIPR model the total flux of products is ejected into a solid angle close to prepared direction of the symmetry axis **â**. A consequence of this tight vector correlation is that the angular distribution in the O-frame $G(\gamma_a)$ is proportional to the orientation dependent integral reaction cross section. According to the best fit trial function for $G(\gamma_a)$ displayed in the upper panel of Figure 10 most products are formed at $\gamma_a = 180°$, that is, if the C−I axis is antiparallel to the relative velocity **V** and the flux of K atoms encounter preferentially the I-end.

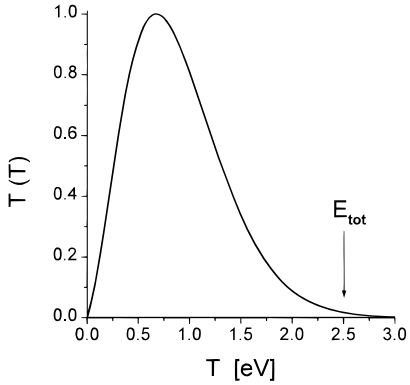

Figure 11. Translational energy distribution for the dominant products in the O-frame.

With decreasing angle the reaction probability rapidly declines and is minimal at a very low level if the symmetry axis is parallel to **V** and the K atoms approach favorably the phenyl end. Obviously, the bulky phenyl ring prevents the K atoms from approaching the I atom close enough to initiate the reaction and the formation of products is efficiently hindered. The head versus tail asymmetry of the reaction probability amounts to

$$\sigma_{\text{head}}/\sigma_{\text{tail}} = \frac{G(180°)}{G(0°)} = 28 \tag{27}$$

$G(\gamma_a)$ is tightly related to the steric opacity function $P_{\text{st}}(b,\cos\gamma_c)$ which describes the probability that the reaction is initiated if the distance between the centers of the two reagents falls below the critical distance R_c (reaction shell). γ_c denotes the bond angle C_6H_5-I-K of the collision complex and b is the impact parameter. With assumption (i) and a spherical reaction shell with radius R_c one obtains

$$G(\gamma_a) = \int_0^{R_c}\int_{2\pi} P_{\text{st}}(b, \cos\gamma_c)\, b\, \mathrm{d}b\, \mathrm{d}\phi_b \tag{28}$$

with

$$\cos\gamma_c = (1 - b^2/R_c^2)^{1/2}\cos\gamma_a + b/R_c \sin\gamma_a \cos(\phi_b - \phi_a) \tag{29}$$

where ϕ_b is the azimuthal angle of the trajectory. Insertion of the b independent trial function

$$P_{\text{st}}(\cos\gamma_c) = \exp[-(1 + \cos\gamma_c)/0.6] \tag{30}$$

furnishes an excellent fit of $G(\gamma_a)$ as illustrated by the dotted line in Figure 10 (upper panel). The opacity function is depicted in the lower panel of Figure 10. The reaction probability steeply descends with the bond angle γ_c and becomes insignificant near the collinear conformation $K-C_6H_5-I$. The apex angle of a representative cone-of-acceptance defined by the full width at half maximum of the opacity function amounts to 110°.

After initiation of the reaction, the C−I bond explodes and repulsive energy R is released and converted to kinetic energy T of the receding products in the O-frame. Assuming $R = T$ and using eq 23, the distribution $\mathcal{T}(T)$ of the kinetic energy can be deduced from the velocity distribution $W(w)$ via

$$\mathcal{T}(T) \propto W(w)/w \tag{31}$$

The result is displayed in Figure 11; the most probable and mean kinetic energy amount to 0.68 and 0.90 eV, respectively. Of course, these energies are lower limits for R because a fraction of the released energy might be vested in the internal degrees of freedom of the products.

A quantitative, theoretical interpretation of the findings in terms of chemical forces is not yet possible due to the lack of precise potential energy surfaces. On the lowest level the phenyl radical could be considered as a quasiatom similar to methyl in reactions with CH_3I, but the large number of electrons is still a severe obstacle and no dramatic breakthrough can be expected for the near future. However, a qualitative rationale of the impulsive mechanism and steric effects can be given on the basis of the harpooning mechanism and primitive molecular orbital (MO) arguments analogous to the reaction $K + CH_3I \rightarrow KI + CH_3$.[18] In the latter the valence electron of K is transferred at a critical distance to a stronly antibonding σ^*-type orbital (along the I−C bond). This creates a repulsion and the molecule rapidly decays into CH_3 and I^-. For $K + C_6H_5I$, the situation is somewhat different due to the presence of the π-type MOs localized at the carbon ring whose energies are well below the one of the σ^*-type MO. The valence electron of the K atom will first populate one of the lowest unoccupied MOs of C_6H_5I, the nonbonding a_2, or the weakly antibonding b_1 π-type MOs of the carbon ring.[29] Population of the orbitals leads to repulsion and the $C_6H_5I^-$ starts separating. Due to the increasing C−I distance the overlap between the AOs forming the σ^* MO decreases and the MO energy steeply descends and eventually falls below the energies of the a_2 and b_1 MOs. Then, near the intersections the electron can migrate to the strongly antibonding σ^* MO, and analoguous to CH_3I^-, the anion dissociates rapidly into $C_6H_5 + I^-$. On the basis of MO computations, Han and co-workers[21] have proposed a similar scheme for the reaction $Ba + C_6H_5X \rightarrow BaX + C_6H_5$ (X = Cl, Br, I).

In the harpooning model steric effects may arise from a bulky, nonreactive group which at some orientations rejects the atom before it reaches the critical distance or, if this distance is reached, from the angle dependence of the potential matrix element which couples the ionic and covalent potential curves of the reagents and governs the electron jump probability. The steep decrease of the steric opacity function near $\gamma_c = 180°$ where the I atom is not shielded by the phenyl group and the very small reaction probability for $\gamma_c = 0°$ suggest that both schemes may play an important role.

Due to the limited experimental information, only a few remarks about the minor component are possible at the present state. We find that the unknown products move in the CM frame practically with the stripping velocity of KI sharply collimated into the forward direction. On the other hand in the O-frame they move extremely slowly and the angular distribution $G^m(\gamma)$ indicates backward scattering. The steric effect of this component could not be determined precisely and is presumably known only with respect to the sign. The estimate, however, indicates preferential formation of products for attacks to the phenyl-end. Since the minor component moves practically with the stripping velocity of KI this product is the most likely candidate. It may be formed by a second mechanism involving a soft dissociation of the C-I bond. The mechanism could be similar to the one postulated for the reaction $K + ICl \rightarrow KCl + I$.[3] The observed fast and slow KCl components were attributed to the existence of two different electronic states of ICl^- correlating with the degenerate separated atom states. Subsequent to the electron jump one state dissociates with substantial the other with insignificant energy release in the O-frame. Deviating from ICl^-, the asymptotic state of $I^- + C_6H_5$ is not degenerate, but there are the two closely lying electronic states of the $C_6H_5I^-$ anion. Their population and subsequent dissociation via the repulsive σ^* MO could well lead to different energy releases.

Slow KI could be formed also by a chemiluminescent channel with electronically excited phenyl. Population of the lowest excited state ($\tilde{A}^2B_1$) would consume 2.4 eV and leave only little energy for the translational degree of freedom of the separating products. Further candidates are processes which do not form KI, and thus the coincidence of the product velocity with the stripping velocity of KI would be accidental. For example, at the collision energy of $E_{tr} = 1.9$ eV, the endoergic reaction channel forming the products C_6H_5 K + I is open. Since the energetic threshold is close to our collision energy, only little energy would be available for the separation of products. Also collisional excitation of the ^2P state of K is possible and would absorb 1.6 eV. The scattered K atoms would be slow particularly if the process is coupled with rovibronic excitation of iodobenzene. Further work is in progress to settle the identity of the minor component.

Acknowledgment. Support of this work by the Deutsche Forschungsgemeinschaft (SFB 216, P5) is gratefully acknowledged.

Appendix 1

O ↔ CM transformation of variables

$$u = (w^2 + u^2_{\text{strip}} + 2wu_{\text{strip}} \cos \gamma)^{1/2}$$

$$\cos \vartheta = \frac{w \cos \gamma + u_{\text{strip}}}{u}$$

$$\varphi = \phi$$

$$w = (u^2 + u^2_{\text{strip}} - 2uu_{\text{strip}} \cos \vartheta)^{1/2}$$

$$\cos \gamma = \frac{u \cos \vartheta - u_{\text{strip}}}{w}$$

$$\phi = \varphi$$

Appendix 2

Trial functions and best fit parameters

$$G(\gamma) = \exp[c_1(\pi - \gamma)^{c_2}]$$

$$W(w) = w^2 \exp\left[-\left(\frac{w - w_0}{w_1}\right)^2\right]$$

$$G^m(\gamma) = (1 - \cos \gamma)^2$$

$$W^m(w) = a^m w^2 \exp\left[-\left(\frac{w}{w_2}\right)^2\right]$$

$$f_{10}(\gamma) = \begin{cases} [\sin(\pi - \gamma)]^S & \gamma \geq \pi/2 \\ 1 & \gamma < \pi/2 \end{cases}$$

$$f_{11}(\gamma) \equiv 1$$

$$w_0 = 437.09 \text{ m/s}; \quad w_1 = 248.13 \text{ m/s}; \quad w_2 = 105.39 \text{ m/s};$$
$$c_1 = -0.544\,70; \quad c_2 = 1.5796; \quad a^m = 0.343\,30;$$
$$s = 0.433\,16$$

References and Notes

(1) Loesch, H. J. *Annu. Rev. Phys. Chem.* **1995**, *46*, 555.

(2) (a) Loesch, H. J. Remscheid, A. *J. Chem. Phys.* **1990**, *93*, 4778. (b) Loesch, H. J.; Remscheid, A. *J. Phys. Chem.* **1991**, *95*, 8194.

(3) (a) Loesch, H. J.; Möller, J. *J. Chem. Phys.* **1992**, *97*, 9016. (b) Loesch, H. J.; Möller, J. *J. Phys. Chem.* **1993**, *97*, 2158.

(4) van Leuken, J. J.; Bulthuis, J.; Stolte, S.; Loesch, H. J. *J. Phys. Chem.* **1995**, *99*, 13583.

(5) (a) Friedrich, B.; Herschbach, D. R.; Rost, J.-M.; Rubahn, H. G.; Renger, M.; Verbeek, M. *J. Chem. Soc., Faraday Trans.* **1993**, *89*, 1539. (b) Friedrich, B.; Slenczka, A.; Herschbach, D. R. *Can. J. Chem.* **1994**, *72*, 897 (c) Friedrich, B. *Int. Rev. Phys. Chem.* **1995**, *14*, 113.

(6) Block, P. A.; Bohac, E. J.; Miller, R. E. *Phys. Rev. Lett.* **1992**, *68*, 1303.

(7) Durand, A.; Loison, J. C.; Vigué, J. *J. Chem. Phys.* **1994**, *101*, 3514.

(8) Friedrich, B.; Rubahn, H.-G.; Sathyamurthy, N. *Phys. Rev. Lett.* **1992**, *69*, 2487.

(9) (a) Bazalgette, G.; White, R.; Loison, J. C.; Trénec, G.; Vigué, J. *Chem. Phys. Lett.* **1995**, *244*, 195. (b) Bazalgette, G.; White, R.; Trénec, G.; Audouard, E.; Bchner, M.; Vigué, J. *J. Chem. Phys.* **1997**. Submitted for publication.

(10) Oudejans, L.; Miller, R. E. *J. Phys. Chem.* **1995**, *99*, 13670.

(11) (a) Harren, F.; Parker, D. H., Stolte, S. *Comments At. Mol. Phys.* **1991**, *26*, 109. (b) Bulthuis, J.; van Leuken, J. J.; Stolte, S. *J. Chem. Soc., Faraday Trans.* **1995**, *91*, 205.

(12) Loesch, H. J.; Bulthuis, J.; Stolte, S.; Durand, A.; Loison, J. C.; Vigué, *Journal of Europhysics News* **1996**, *27*, 12.

(13) Möller, J. Ph.D. Thesis, Universität Bielefeld, Bielefeld, Germany, 1997.

(14) Entemann, E. A.; Kwei, G. H. *J. Chem. Phys. B* **1971**, *55*, 4879.

(15) (a) Busalla, A.; Blum, K. *J. Phys. Chem.* **1997**, *101*, 7476. (b) Ostrawsky, C.; Blum, K.; Gillan, C. *J. Phys. B* **1995**, *28*, 2269.

(16) Kuntz, P. J. *Trans. Faraday Soc.* **1970**, *66*, 2980; *Mol. Phys.* **1972**, *23*, 1035.

(17) (a) Kwei, G. H.; Norris, J. A.; Herschbach, D. R. *J. Chem. Phys.* **1970**, *52*, 1317. (b) Rulis, A. M.; Bernstein, R. B. *J. Chem. Phys.* **1972**, *57*, 5497.

(18) Herschbach, D. R. *Adv. Chem. Phys.* **1966**, *10*, 319.

(19) Brooks, P. R. *Science* **1976**, *193*, 11.

(20) Parker, D. H.; Bernstein, R. B. *Ann. Rev. Phys. Chem.* **1989**, *40*, 561.

(21) Han, K.-L.; He, G.-Z.; Lou, N.-Q. *Chem. Phys. Lett.* **1993**, *203*, 509.

(22) Bulthuis, J.; Möller, J.; Loesch, H. J. *J. Phys. Chem.* **1997**, *101*, 7684.

(23) Loison, J. C.; Durand, A.; Bazalgette, G.; White, R.; Audouard, E.; Vigué, J. *J. Phys. Chem.* **1995**, *99*, 13591.

(24) Schmeling, R. Diplomarbeit, Universität Bielefeld, Bielefeld, Germany, 1997.

(25) (a) Maltz, C.; Weinstein, N. D.; Herschbach, D. R. *Mol. Phys.* **1972**, *24*, 133. (b) Hsu, D. S. Y.; Herschbach, D. R. *Discuss. Faraday Soc.* **1973**, *55*, 116.

(26) A simple fixed velocity transformation of the TOF profiles provides a nearly congruent contour map except for the central region which exhibits a plateau rather than an additional structure.

(27) Riley, S. J.; Siska, P. E.; Herschbach, D. R. *Faraday Discuss. Chem. Soc.* **1979**, *67*, 27.

(28) Bañares, L.; González Ureña, A. *J. Chem. Phys.* **1990**, *93*, 6473.

(29) Jordan, K. D.; Michejda, J. A.; Burrow, P. D. *J. Am. Chem. Soc.* **1976**, *98*, 7189.

(30) Mirri, A. M.; Caminati, W. *Chem. Phys. Lett.* **1971**, *8*, 409.

(31) Le Fèvre, R. J. W.; Narajana Rao, D. A. A. S. *Austr. J. Chem.* **1955**, *8*, 140.

(32) *CRC Handbook of Chemistry and Physics*, 55th ed.; Weast, R. C., Ed.; CRC Press: Cleveland, OH, 1975.

(33) Whiffen, D. H. *J. Chem. Soc.* (*London*) 1956, 1350.

(34) Clark R.; McCaffery, A. J. *J. Phys. Chem.* **1977**, *81*, 1918.

(35) The parameter $\bar{\omega} = d|\mathcal{E}|/\bar{C}_0$ is typical for the electric interaction energy: $\bar{C}_0 = 0.5(B_0 + C_0)$ denotes the mean rotational constant for rotations perpendicular to the symmetry axis.